HHS Public Access

Author manuscript

Ann Plast Surg. Author manuscript; available in PMC 2022 December 01.

Published in final edited form as:

Ann Plast Surg. 2021 December 01; 87(6): e153–e162. doi:10.1097/SAP.0000000000002965.

Transforming the degradation rate of β-tricalcium phosphate bone replacement using 3D printers

Chen Shen, MSci, MD[1,2], **Maxime M. Wang, MD MSci**[1,2], **Lukasz Witek, MSci PhD**[1,3], **Nick Tovar, PhD DDS**[1], **Bruce N. Cronstein, MD**[4], **Andrea Torroni, MD**[2], **Roberto L. Flores, MD**[2], **Paulo G. Coelho, DDS PhD**[1,2,5]

[1]Department of Biomaterials & Biomimetics, NYU College of Dentistry, 433 1st Avenue, New York NY 10010

[2]Hansjörg Wyss Department of Plastic Surgery, NYU Langone Health, 307 E 33rd St, New York NY 10016

[3]Department of Biomedical Engineering, NYU Tandon School of Engineering, 6 MetroTech Center, Brooklyn NY 11201

[4]Department of Medicine, NYU Langone Health, 550 1st Avenue, New York NY 10016

[5]Department of Mechanical Engineering, NYU Tandon School of Engineering, 6 MetroTech Center, Brooklyn NY 11201

Abstract

Background: β-tricalcium phosphate (β-TCP) is one of the most common synthetic bone grafting materials utilized in craniofacial reconstruction, however it is limited by a slow degradation rate. The aim of this study was to leverage 3D-printing to accelerate the degradation kinetics of β-TCP.

Methods: Twenty-two one-month-old New Zealand White rabbits underwent creation of calvarial and alveolar defects, repaired with 3D-printed β-TCP scaffolds coated with 1,000 μM of osteogenic agent dipyridamole. Rabbits were sacrificed after 2, 6, and 18 months post-surgical intervention. Bone regeneration, scaffold degradation, and bone mechanical properties were quantified.

Results: Histology analysis confirmed the generation of vascularized and organized bone. Micro CT analysis from 2 to 18 months, demonstrated decreased scaffold volume within calvarial (23.6% ± 2.5%, 5.1% ± 2.2%; $p < 0.001$) and alveolar (21.5% ± 2.2%, 0.2% ± 1.9%; $p < 0.001$) defects, with degradation rates 54.6%/year and 90.5%/year, respectively. Scaffold-inducted bone generation within the defect was volumetrically similar to native bone in the calvarium (55.7% ± 6.9% vs. 46.7% ± 6.8%; $p = 0.064$) and alveolus (31.4% ± 7.1% vs. 33.8% ± 3.7%; $p = 0.337$). Mechanical properties between regenerated and native bone were similar.

Corresponding Author: Lukasz Witek, MSci, PhD 433 1st Ave, Room 842, New York, NY 10010, (212) 998-9269, lw901@nyu.edu.

Disclosures: Drs. Paulo G. Coelho and Bruce N. Cronstein have filed a patent about the use of tissue repair devices and scaffolds (#: US20150150681A1). Dr. B. Cronstein holds patents numbers 5,932,558; 6,020,321; 6,555,545; 7,795,427.

Conclusions: Our study demonstrates an improved degradation profile and replacement of absorbed β-TCP with vascularized, organized bone through 3D printing and addition of an osteogenic agent. This novel additive manufacturing and tissue engineering protocol has implications to the future of craniofacial skeletal reconstruction as a safe and efficacious bone tissue engineering method.

Introduction/Background

β-tricalcium phosphate (β-TCP), one of the most common synthetic bone grafting products, is frequently utilized in craniofacial reconstruction. β-TCP is a porous osseoconductive bioactive ceramic compound which has similar mechanical properties as cancellous bone.(1–4). The graft material is biocompatible and may be used as granules or implantable solid shapes, with numerous applications in spine, orthopedic, and craniofacial surgery,(1, 5–7) but it is notably brittle and slow to resorb.(8)

Although solid β-TCP is absorbed over time, a relatively slow degradation rate predisposes this product to exposure, infection, and fracture. Clinical trials of β-TCP products in the craniofacial skeleton report the graft material lasting several years,(9–12) with similar findings noted in animal models.(13–16) Of note, highly porous scaffolds with bone marrow aspirate, protein-rich plasma, or stem cell cultures have the highest degradation rates,(17–22) suggesting the utility of tissue engineering principles in transforming the degradation rate while maintaining the necessary mechanical stability of solid β-TCP implants in craniofacial surgery. Balancing the needs of osteogenesis, mechanical stability of the scaffold and degradation kinetics has significant importance in the growing face, as bone implants should ideally grow and remodel with the patient.

Our tissue engineering laboratory has successfully leveraged 3D printers to manufacture 3D-printed bioactive ceramic (3DPBC) scaffolds composed of β-TCP in an architecture which balances the needs of rigidity with efficient vascular ingrowth, osteogenesis, and degradation kinetics.(23–26) In these studies, we coated the scaffolds with dipyridamole (DIPY), an indirect adenosine 2A receptor ($A_{2A}R$) agonist with pro-osteogenic activity,(27–31) further optimizing the osteogenic capabilities of our bioceramic scaffolds.(23) DIPY was selected for its regenerative equivalence to recombinant human bone morphogenic protein 2 (rhBMP-2) but without premature suture fusion or osteolysis.(24, 26) Long-term investigation in a growing craniofacial rabbit model showed equivalent bone regeneration to autologous bone graft without ectopic bone growth, premature suture fusion, or facial asymmetry.(32)

We hypothesize that utilizing these 3DPBC-DIPY scaffolds will accelerate the degradation rate of β-TCP, while regenerating vascularized, mature bone with mechanical and histologic properties similar to those of native bone. This long-term animal study of immature rabbits through the time of facial maturity reports on the new degradation kinetics profile achievable through this novel manufacturing and tissue engineering protocol.

Methods

All 3DPBC scaffolds were composed of 100% β-TCP, designed via computer assisted design (CAD) (RoboCAD 4.5; 3D Inks LLC, Tulsa, OK, USA), and constructed using a custom-built 3D direct-write micro-printer system (3D Inks LLC, Tulsa, OK, USA). Colloidal gel ink was formulated to achieve a solid volume fraction of ~46% by blending ceramic powder, ammonium polyacrylate, deionized water, hydroxypropyl methylcellulose, and polyethlenimine.(24) Calvarial scaffolds were printed layer-by-layer in paraffin oil as a 10 mm-diameter cylindrical lattice with 250 μm struts and 500 μm pore spacing, (24, 26) which was previously demonstrated to result in maximal bone regeneration and effective scaffold degradation.(26) Alveolar scaffolds were printed in a 3.5 × 3.5 × 3.5 mm rectangular lattice in a similar strut and pore spacing.(24) Printed scaffolds were then sintered to 1100°C to densify the constructs and remove impurities.(33)

Prior to implantation, scaffolds were loaded by immersion in 2% bovine collagen solution (Collagen I, Bovine; Corning Inc., Corning, NY, USA) as a carrier and then coated with 1,000 μM DIPY.(23, 25, 26) Where the concentration was demonstrated in previous studies to result in favorable bone regeneration.(23, 24, 26)

All experiments were approved by the NYU School of Medicine Institutional Animal Care and Use Committee (IACUC) and were performed in accordance with their standards. Twenty-two one-month-old (immature) New Zealand White rabbits underwent creation of unilateral right-sided 10 mm calvarial(26) and 3.5 × 3.5 mm alveolar defects,(25) which were all repaired using custom DIPY-3DPBC scaffolds (Figure 1).

Following general anesthesia and aseptic preparation of the site over the calvarium, dissection was performed down to the periosteum. A 10 mm internal diameter trephine were used to create the full-thickness defects, located 2 mm posterior and lateral to the coronal and sagittal sutures, respectively. Preservation of the dura was confirmed after craniotomy. The cranial defect was repaired with a DIPY-3DPBC scaffold which completely fit and filled the defect such that circumferential abutment of the scaffold to the surrounding bone was achieved.

Next, the animal was repositioned and attention was turned to the alveolus. Soft tissue and periosteum were dissected to visualize the maxilla, alveolar ridge, and maxillary suture. Using a 3D printed template, a uniform 3.5×3.5 mm full-thickness defect was created using an oral surgery burr 2 mm posterior to the maxillary suture. Can was taken not to violate the maxillary sinus. The alveolar defect was repaired with a DIPY-3DPBC scaffold which completely fit and filled the defect such that abutment of the scaffold to the mesial, distal and superior bone was achieved.

Subcutaneous analgesic and antibiotic were administered post-operatively, and animals were given food *ad libitum* without restrictions to their activity. Animals were euthanized via anesthetic overdose at 2 months (n = 6), 6 months (n = 8), and 18 months (n = 8), with the latter two timepoints being beyond completion of craniofacial growth conservatively estimated at 28–30 weeks (Gilsanz 1988, Masoud 1986).

Samples were then partitioned to isolate the region surrounding with calvarial or alveolar defects. High-resolution micro computed tomography (μCT, Scanco medical, Basserdorf, Germany) images were acquired at 18 μm slice resolution for specific areas of interest within those sections. These μCT sections were then reconstructed in *Amira* (Version 6.3, Visage Imaging GmbH, Berlin, Germany) to create 3D digital renderings of the defects to analyze for bone regeneration and scaffold degradation. Areas of bone were distinguished from scaffold by image thresholding using Hounsfield units (24, 26). Volumes of bone (BV) and of scaffold (SV) were calculated as proportions of the total volume (TV) of the defect (BV/TV and SV/TV, respectively). Contralateral 10 mm calvarial discs and 3.5 × 3.5 mm alveolar sections were also isolated and quantified for native bone volume fraction for comparison. Un-implanted scaffolds were also scanned and reconstructed to establish a $t = 0$ time point to evaluate scaffold degradation kinetics. μCT analysis was conducted by a single, blinded investigator (CS).

Scaffold degradation profile was constructed by plotting percent change in scaffold volume fraction over time. An inverse exponential function was fitted to the degradation curves and used to calculated yearly degradation rate of the 100% β-TCP scaffolds.

After μCT imaging, samples were dehydrated in a series of 70–100% ethanol (EtOH) solutions and embedded in methyl methacrylate resin. The embedded blocks were subjected to serial sectioning with a diamond saw (Isomet 2000, Buehler Ltd., Lake Bluff, IL, USA) with individual slices glued onto acrylic slides and ground on a grinding machine (Metaserv 3000, Buehler, Lake Bluff, IL, USA) under continuous water irrigation with a series of SiC abrasive paper until a thickness of 100 μm was achieved. The slides were then stained using Stevenel's blue and van Gieson's picrofuchsin to differentiate between bone, scaffold, and soft tissue. These samples were imaged at low magnification (1×, 10 μm/pixel) using pathology slide scanner (Aperio Technologies, Vista, CA, USA) and qualitatively evaluated for suture patency, bone organization, ectopic bone formation, scaffold fragmentation, and histologic evidence of excess inflammation or morbidity secondary to surgery.

A second set of slides were prepared in similar fashion for nanoindentation but with the additional step of sequential 9 to 1 μm diamond suspension (Buehler, Lake Bluff, IL) polishing for scratch removal. Nanoindentation testing was performed using a nanoindenter (Hysitron TI 950, Minneapolis, MN) equipped with a Berkovich diamond three-sided pyramid probe/tip.(24) A loading profile with peak load of 300 μN at a rate of 60 μN/s was applied, with a holding period of 10 seconds and unloading period of 2 seconds. For each specimen, indentation (16 points, 5 μm apart in a 4 × 4 grid) was performed within scaffold interstices at sites of newly regenerated bone and within unoperated native bone outside of the scaffold, the latter of which served as an internal control. Regions of bone were chosen by visualization with light microscopy. The indentation protocol generated a force-displacement curve via TriboScan software with slopes that yielded the reduced modulus (E_r) and hardness (H) of bone tissue using the formulae:

$$E_r = \frac{\sqrt{\pi}}{2\sqrt{A(h_c)}} \times S$$

$$H = \frac{P_{max}}{A(h_c)}$$

where $A(h_c)$ is the contact area at peak load (P_{max}) and S is stiffness.(24)

Sample size was determined *a priori* using power analysis based on preliminary 8-week experiments. Analysis revealed n = 6 per group was necessary to achieve a power >80% to detect 25% mean differences in bone volume regeneration relative to control with a standard deviation of 15% at an alpha (α) of 0.05. All μCT data was assessed for normality using the Shapiro-Wilk test ($p > 0.05$) prior to further analysis. Bone volume percentage and scaffold volume percentage at 18 months were compared between scaffold-repaired defects and contralateral native bone using a generalized linear mixed model (GLMM) in SPSS (Version 26.0, IBM Corp., Armonk, NY). All data is presented as a mean value with corresponding 95% CI. Temporal analysis of bone regeneration from 2 months to 18 months, reduced elastic modulus, and hardness were also analyzed using a GLMM.(24)

Results

Amira software reconstruction was used to visualize and quantify new bone formation and scaffold presence. At 18 months, mean bone volume percentage (BV/TV) within the calvarial and alveolar defects were 55.7% ± 6.9% and 31.4% ± 7.1%, respectively. Bone volume percentage in the calvarium was significantly increased compared to that at 2 months (25.8% ± 7.9%, $p < 0.001$) and no different at 6 months (53.9% ± 6.9%, $p = 0.705$) or compared to native bone density (46.7% ± 6.8%, $p = 0.064$) (Figure 2c). Bone volume percentage in the alveolus was no different compared to that at 2 months (28.4% ± 8.2%, $p = 0.566$), significantly decreased from 6 months (52.9% ± 7.1%, $p < 0.001$), and no different from native bone density (33.8% ± 3.7%, $p = 0.337$) (Figure 2c).

Mean scaffold volume percentage (SV/TV) within the calvarial and alveolar defects at 18 months were 5.1% ± 2.2% and 0.2% ± 1.9%, respectively. Scaffold volume percentage in the calvarium was significantly decreased compared to that at 2 months (23.6% ± 2.5%, $p < 0.001$) and at 6 months (15.2% ± 2.2%, $p < 0.001$) (Figure 3c). Scaffold volume percentage in the alveolus was significantly decreased compared to that at 2 months (21.5% ± 2.2%, $p < 0.001$) and at 6 months (6.7% ± 1.9%, $p < 0.001$) (Figure 3c). The annual degradation rates of 100% β-TCP scaffolds in the calvarium and alveolus were calculated to be 54.6% and 90.5%, respectively (Figure 4).

In the calvarium, regenerated bone and native bone had statistically homogenous elastic moduli (12.6 GPa ± 1.8 GPa vs. 13.2 GPa ± 1.8 GPa, $p = 0.616$) and hardness (0.54 GPa ± 0.06 GPa vs. 0.53 GPa ± 0.06 GPa, $p = 0.812$) (Fig. 5a and 5b). In the alveolus, regenerated bone and native bone had similar elastic moduli (11.7 GPa ± 1.5 GPa vs. 11.3 GPa ± 1.5 GPa, $p = 0.707$) and hardness (0.64 GPa ± 0.05 GPa vs. 0.66 GPa ± 0.05 GPa, $p = 0.703$) (Figure 5c and 5d).

Histology of tissue samples from animals after 18 months of scaffold implantation revealed vascularized and organized bone without suture fusion (Figure 6). Neither evidence of ectopic bone formation nor inflammatory cell infiltration was visualized.

Discussion

We present a novel tissue engineering and manufacturing protocol to transform the degradation profile of β-TCP for more efficacious use in pediatric patients. Our study demonstrates an acceleration of β-TCP degradation to 55–90%/year through 3D printing and addition of dipyridamole (DIPY). Absorbed β-TCP was replaced by vascularized, organized bone, with histologic and mechanical properties similar to native bone and without damage noted to the growing suture.

Standard of care for these patients remains autologous bone.(34–37) Limitations of bone grafting include donor site morbidity, bone resorption, limited quantity and shape of bone stock, and difficulty shaping bone grafts into complex 3D forms to reconstruct craniofacial defects.(35, 37–42) Limitations to current standard of care for bony reconstruction of the pediatric craniofacial skeleton inspire development of alternative interventions, especially in the field of tissue engineering. Utilizing computer aided design/manufacturing (CAD/CAM) software would enable surgeons to precisely design and manufacture scaffolds to the specifications of a patient's craniofacial defect.(17, 25, 43, 44)

β-TCP, in particular, provides structure and rigidity, promotes osteocyte migration, and is biocompatible and biodegradable, making it the ideal synthetic bone replacement material for tissue engineering.(1, 5–8, 45) Historically, scaffolds designs have been comprised of hydroxyapatite (HA) as bulk material.(25) Though relative to β-TCP, HA has high initial compressive strength and low resorption kinetics *in vivo* (1–2% per year at five years post-implantation), limiting scaffold replacement by bone over time.(46) As a result, β-TCP ceramic was developed, with biocompatibility and osteoconductivity similar to HA but with an increased degradation rate.(46, 47) Similar attempts in designing biodegradable, biocompatible scaffolds for bone tissue engineering led to the use of polymers such as collagen, polycaprolactone (PCL), poly(glycolic acid) (PGA), and poly(lactic acid) (PLA), but these natural and synthetic polymers are not ideal for bone tissue engineering due to inferior mechanical properties compared to bioceramics.(48–50)

Long-term growth and development of the craniofacial skeleton must also be carefully considered since even standard of care bone grafting may lead to potential growth restriction due to multiple revision surgeries (51) or secondary surgery due to bone graft absorption. Therefore, our novel tissue engineering protocol sought to accelerate the slow degradation rate of β-TCP to facilitate timely replacement by new bone tissue that would grow and remodel with the patient.

Additive manufacturing, also known as 3D printing, has the ability to create personalized scaffolds based on clinical imaging and offers a valuable approach to fit-and-fill patient-specific bony defects. Traditional scaffolds were composed of bulk material such as HA, (50) but 3D printing allows for the design of porous scaffolds that act temporary void

fillers like bulk scaffolds with the added benefit of pores that behave as healing chambers, guiding osteoconduction from the walls of the defect into pores via an intramembranous-like healing pathway and filling the scaffold lattice structure with woven bone.(52) Our calvarial scaffolds had a porosity of 40% and alveolar scaffolds had a porosity of 32%. Based on prior literature, these scaffolds would have an elastic modulus ranging from 10–20 GPa, similar to that of bone of the same porosity.(53) In terms of compressive strength, however, porous β-TCP scaffolds are inferior to porous HA scaffolds, both of which are inferior to bone of the same porosity.(53) This finding, though, is only important when designing load-bearing scaffolds, which is less of an issue in our calvarial and alveolar models as those locations are generally non-load-bearing. Thus, our porous β-TCP scaffolds were designed to optimize regenerate bone and degradation.

A review of literature of *in vivo* translational studies exploring β-TCP degradation revealed several tissue engineering methods that altered the degradation profile of this biomaterial (Table 1). A general consensus is β-TCP degradation rate should match osteogenesis rate.(54, 55) Assuming equivalent osteogenic potential, premature degradation leads to incomplete healing(56) and slow degradation leads to increased risk of inflammation, infection, and rejection.(57, 58) Overall, seeding β-TCP scaffolds with bone marrow-derived stem cells (BMSCs) slows degradation,(54, 55) while integration of osteogenic agent acceleration degradation.(59–61) Some exceptions have been reported, possibly due to increased vascularization promoting degradation via hydrolysis from tissue fluid despite seeding of BMSCs;(62) growth factors stimulating already seeded stem cell proliferation, collagen network formation, and mineral apposition delaying dissolution and degradation;(55) and presence of BMSCs reducing the inflammatory response to slow-degrading scaffolds.(58) Contrarily, some studies in craniofacial skeleton using BMSC-seeded scaffolds found faster degradation when compared to plain scaffold on the order of near complete degradation at 3 and 8 months. These studies included an adult canine orbital wall (57) and mandible (56) models, respectively. A limit of this review is lack of consistent defect model and measurement of degradation kinetics to compare with the rates calculated in this study. Although, scaffold design and biomaterial property may play a bigger role in degradation rate than the presence or absence of BMSCs and osteogenic agents, these tissue engineering principles can help achieve balance between scaffold degradation and bony regeneration, for a scaffold that degrades too rapidly would hinder the formation of bridging bone across the defect. In our study, addition of osteogenic agent DIPY promoted new bone formation without damage to sutures or ectopic bone growth and is, thus, another safe and efficacious bone tissue engineering method.

Remodeling and pneumatization of regenerated bone were evident in the alveolus. At 6 months, regenerated alveolar bone is denser than unoperated bone,(32) but 3D reconstruction in this current study demonstrated decreased in regenerated bone volume percentage from 6 months to 18 months, culminating at similar bone density between regenerated and native contralateral alveolar bone. In addition, regenerated alveolar bone was functionally similar to native bone in terms of mechanical properties. This morphologic difference yet mechanical similarity has been noted in mandibular defect models.(56) In a similar study published by our group, no significant difference was noted in bone volume between calvarial and alveolar defects repaired with 3DPBC-DIPY scaffolds and autologous

bone graft at 6 months.(32) Furthermore, regenerated bone density was significantly increased compared to native contralateral unoperated bone density yet with similar mechanical properties. Therefore, these results imply that regenerated alveolar bone tissue eventually remodels to native bone density without detriment to function when given enough time. Degradation rate and bone tissue properties were different between calvarial bone and alveolar bone, highlighting the metabolic and mechanical heterogeneity in the craniofacial skeleton that is important to consider when applying tissue engineering principles to craniofacial reconstruction. Thus, we believe studies beyond our 18-month period will demonstrate regenerated calvarial bone undergoing remodeling and pneumatization like regenerated alveolar bone. Longer-term studies of both alveolar and calvarial models, however, are required to draw definitive conclusions.

A limitation of this study is the lack of a positive control population with standard of care bone grafting. Previous research has already reported on the equivalent efficacy of our DIPY-3DPBC scaffolds when compared autologous bone grafting in a growing animal model.(32) In addition, these 3DPBC scaffolds, with and without DIPY, are able to repair larger critically-sized defects beyond the ones used in this study as evidenced by prior studies published by our group.(23, 25)

Degradation rate of 3DPBC scaffolds coated in collagen without DIPY was not analyzed in this study. Although no direct conclusions can be made of the role of DIPY in degradation of these scaffolds, previous studies have determined that DIPY significantly improves bone regenerative capacity of 3DPBC scaffolds. (23) DIPY, therefore, ensures appropriate replacement of a rapidly degrading scaffold with vascularized, organized bone. By balancing biomaterial degradation and bone regeneration, 3DPBC-DIPY scaffolds provide a more representative therapeutic device in this bone tissue engineering model.

Additionally, while histologic and mechanical analysis revealed normal bone density and mechanical properties, micro-CT reconstruction of the alveoli revealed a gross architecture qualitatively different from the contralateral side, the clinical implications of which are not known. These differences may be resolved by a longer period of observation for bony remodeling. It is important to note that the elastic moduli and hardness of the generated bone is comparable to native bone. Nevertheless, the qualitative differences in bony architecture between the native and generated bone underscore the importance of the complex balance between osteogenesis, graft resorption, and remodeling integral in successful surgical outcomes. Slow graft absorption may limit bony ingrowth,(38, 63) but rapid graft resorption will lead to graft failure.(38, 64, 65)

Overall, this long-term animal study demonstrated accelerated β-TCP degradation rate using 3DPBC-DIPY scaffolds, while generating vascularized, mechanically stable bone.

Conclusion

The degradation kinetics of β-TCP can be altered through 3D printing and addition of an osteogenic agent. Absorbed β-TCP is replaced by vascularized, organized bone, with histologic and mechanical properties similar to native bone and without damage noted to the

growing suture. This additive manufacturing and tissue engineering protocol has implication to future reconstruction of the craniofacial skeleton, especially as a safe and efficacious method in pediatric bone tissue engineering.

Acknowledgments

Funding: This work was supported by the National Institutes of Health [R33HD090664].

References

1. LeGeros RZ, Lin S, Rohanizadeh R, et al. Biphasic calcium phosphate bioceramics: preparation, properties and applications. J Mater Sci Mater Med 2003;14:201–209 [PubMed: 15348465]
2. Rh Owen G, Dard M, Larjava H. Hydoxyapatite/beta-tricalcium phosphate biphasic ceramics as regenerative material for the repair of complex bone defects. J Biomed Mater Res B Appl Biomater 2018;106:2493–2512 [PubMed: 29266701]
3. Lowe B, Ottensmeyer MP, Xu C, et al. The Regenerative Applicability of Bioactive Glass and Beta-Tricalcium Phosphate in Bone Tissue Engineering: A Transformation Perspective. J Funct Biomater 2019;10
4. Andratschke M, Hagedorn H. First results of frontal sinus obliteration with a synthetic, resorbable and osteoconductive bone graft of ß-tricalcium phosphate. J Laryngol Otol 2017;131:534–540 [PubMed: 28366182]
5. Bucholz RW. Nonallograft osteoconductive bone graft substitutes. Clin Orthop Relat Res 2002:44–52 [PubMed: 11937865]
6. Daculsi G, Laboux O, Malard O, et al. Current state of the art of biphasic calcium phosphate bioceramics. J Mater Sci Mater Med 2003;14:195–200 [PubMed: 15348464]
7. Pryor LS, Gage E, Langevin CJ, et al. Review of bone substitutes. Craniomaxillofac Trauma Reconstr 2009;2:151–160 [PubMed: 22110809]
8. Roberts TT, Rosenbaum AJ. Bone grafts, bone substitutes and orthobiologics: the bridge between basic science and clinical advancements in fracture healing. Organogenesis 2012;8:114–124 [PubMed: 23247591]
9. Bae JH, Kim YK, Kim SG, et al. Sinus bone graft using new alloplastic bone graft material (Osteon)-II: clinical evaluation. Oral Surg Oral Med Oral Pathol Oral Radiol Endod 2010;109:e14–20 [PubMed: 20219580]
10. Bagot d'Arc M, Daculsi G, Emam N. Biphasic ceramics and fibrin sealant for bone reconstruction in ear surgery. Ann Otol Rhinol Laryngol 2004;113:711–720 [PubMed: 15453528]
11. Ciprandi MT, Primo BT, Gassen HT, et al. Calcium phosphate cement in orbital reconstructions. J Craniofac Surg 2012;23:145–148 [PubMed: 22337393]
12. Horch HH, Sader R, Pautke C, et al. Synthetic, pure-phase beta-tricalcium phosphate ceramic granules (Cerasorb) for bone regeneration in the reconstructive surgery of the jaws. Int J Oral Maxillofac Surg 2006;35:708–713 [PubMed: 16690249]
13. Handschel J, Wiesmann HP, Stratmann U, et al. TCP is hardly resorbed and not osteoconductive in a non-loading calvarial model. Biomaterials 2002;23:1689–1695 [PubMed: 11922472]
14. Wiltfang J, Merten HA, Schlegel KA, et al. Degradation characteristics of alpha and beta tri-calcium-phosphate (TCP) in minipigs. J Biomed Mater Res 2002;63:115–121 [PubMed: 11870643]
15. Klein CP, Driessen AA, de Groot K, et al. Biodegradation behavior of various calcium phosphate materials in bone tissue. J Biomed Mater Res 1983;17:769–784 [PubMed: 6311838]
16. Sawada K, Nakahara K, Haga-Tsujimura M, et al. Comparison of three block bone substitutes for bone regeneration: long-term observation in the beagle dog. Odontology 2018;106:398–407 [PubMed: 29557992]
17. Tada H, Hatoko M, Tanaka A, et al. Preshaped hydroxyapatite tricalcium-phosphate implant using three-dimensional computed tomography in the reconstruction of bone deformities of craniomaxillofacial region. J Craniofac Surg 2002;13:287–292 [PubMed: 12000888]

18. Thesleff T, Lehtimäki K, Niskakangas T, et al. Cranioplasty with Adipose-Derived Stem Cells, Beta-Tricalcium Phosphate Granules and Supporting Mesh: Six-Year Clinical Follow-Up Results. Stem Cells Transl Med 2017;6:1576–1582 [PubMed: 28504874]
19. Kaigler D, Avila-Ortiz G, Travan S, et al. Bone Engineering of Maxillary Sinus Bone Deficiencies Using Enriched CD90+ Stem Cell Therapy: A Randomized Clinical Trial. J Bone Miner Res 2015;30:1206–1216 [PubMed: 25652112]
20. Smiler D, Soltan M, Lee JW. A histomorphogenic analysis of bone grafts augmented with adult stem cells. Implant Dent 2007;16:42–53 [PubMed: 17356371]
21. Shayesteh YS, Khojasteh A, Soleimani M, et al. Sinus augmentation using human mesenchymal stem cells loaded into a beta-tricalcium phosphate/hydroxyapatite scaffold. Oral Surg Oral Med Oral Pathol Oral Radiol Endod 2008;106:203–209 [PubMed: 18424115]
22. Bulgin D, Hodzic E. Autologous Bone Marrow-Derived Mononuclear Cells Combined With β-TCP for Maxillary Bone Augmentation in Implantation Procedures. J Craniofac Surg 2017;28:1982–1987 [PubMed: 29088691]
23. Bekisz JM, Flores RL, Witek L, et al. Dipyridamole enhances osteogenesis of three-dimensionally printed bioactive ceramic scaffolds in calvarial defects. J Craniomaxillofac Surg 2018;46:237–244 [PubMed: 29292126]
24. Lopez CD, Coelho PG, Witek L, et al. Regeneration of a Pediatric Alveolar Cleft Model Using Three-Dimensionally Printed Bioceramic Scaffolds and Osteogenic Agents: Comparison of Dipyridamole and rhBMP-2. Plast Reconstr Surg 2019;144:358–370 [PubMed: 31348344]
25. Lopez CD, Diaz-Siso JR, Witek L, et al. Three dimensionally printed bioactive ceramic scaffold osseoconduction across critical-sized mandibular defects. J Surg Res 2018;223:115–122 [PubMed: 29433862]
26. Maliha SG, Lopez CD, Coelho PG, et al. Bone Tissue Engineering in the Growing Calvarium Using Dipyridamole-Coated 3D Printed Bioceramic Scaffolds: Construct Optimization and Effects to Cranial Suture Patency. Plast Reconstr Surg 2019
27. Costa MA, Barbosa A, Neto E, et al. On the role of subtype selective adenosine receptor agonists during proliferation and osteogenic differentiation of human primary bone marrow stromal cells. J Cell Physiol 2011;226:1353–1366 [PubMed: 20945394]
28. Mediero A, Kara FM, Wilder T, et al. Adenosine A(2A) receptor ligation inhibits osteoclast formation. Am J Pathol 2012;180:775–786 [PubMed: 22138579]
29. Mediero A, Perez-Aso M, Cronstein BN. Activation of adenosine A(2A) receptor reduces osteoclast formation via PKA- and ERK1/2-mediated suppression of NFκB nuclear translocation. Br J Pharmacol 2013;169:1372–1388 [PubMed: 23647065]
30. Mediero A, Wilder T, Perez-Aso M, et al. Direct or indirect stimulation of adenosine A2A receptors enhances bone regeneration as well as bone morphogenetic protein-2. Faseb j 2015;29:1577–1590 [PubMed: 25573752]
31. Ishack S, Mediero A, Wilder T, et al. Bone regeneration in critical bone defects using three-dimensionally printed β-tricalcium phosphate/hydroxyapatite scaffolds is enhanced by coating scaffolds with either dipyridamole or BMP-2. J Biomed Mater Res B Appl Biomater 2017;105:366–375 [PubMed: 26513656]
32. Wang MM, Flores RL, Witek L, et al. Dipyridamole-loaded 3D-printed bioceramic scaffolds stimulate pediatric bone regeneration in vivo without disruption of craniofacial growth through facial maturity. Sci Rep 2019;9:18439 [PubMed: 31804544]
33. Witek L, Smay J, Silva NRFA, et al. Sintering effects on chemical and physical properties of bioactive ceramics. Journal of Advanced Ceramics 2013;2:274–284
34. Gentili C, Torre M, Cancedda R. Tissue engineering approaches in skeletal pediatric disorders. Eur J Pediatr Surg 2014;24:263–269 [PubMed: 24952602]
35. Eufinger H, Leppänen H. Iliac crest donor site morbidity following open and closed methods of bone harvest for alveolar cleft osteoplasty. J Craniomaxillofac Surg 2000;28:31–38 [PubMed: 10851671]
36. Liang F, Leland H, Jedrzejewski B, et al. Alternatives to Autologous Bone Graft in Alveolar Cleft Reconstruction: The State of Alveolar Tissue Engineering. J Craniofac Surg 2018;29:584–593 [PubMed: 29461365]

37. Lam S, Kuether J, Fong A, et al. Cranioplasty for large-sized calvarial defects in the pediatric population: a review. Craniomaxillofac Trauma Reconstr 2015;8:159–170 [PubMed: 26000090]
38. Biskup NI, Singh DJ, Beals S, et al. Pediatric cranial vault defects: early experience with beta-tricalcium phosphate bone graft substitute. J Craniofac Surg 2010;21:358–362 [PubMed: 20186087]
39. Weijs WL, Siebers TJ, Kuijpers-Jagtman AM, et al. Early secondary closure of alveolar clefts with mandibular symphyseal bone grafts and beta-tri calcium phosphate (beta-TCP). Int J Oral Maxillofac Surg 2010;39:424–429 [PubMed: 20303237]
40. Oppenheimer AJ, Mesa J, Buchman SR. Current and emerging basic science concepts in bone biology: implications in craniofacial surgery. J Craniofac Surg 2012;23:30–36 [PubMed: 22337370]
41. Francis CS, Mobin SS, Lypka MA, et al. rhBMP-2 with a demineralized bone matrix scaffold versus autologous iliac crest bone graft for alveolar cleft reconstruction. Plast Reconstr Surg 2013;131:1107–1115 [PubMed: 23385986]
42. Banwart JC, Asher MA, Hassanein RS. Iliac crest bone graft harvest donor site morbidity. A statistical evaluation. Spine (Phila Pa 1976) 1995;20:1055–1060 [PubMed: 7631235]
43. Ma H, Feng C, Chang J, et al. 3D-printed bioceramic scaffolds: From bone tissue engineering to tumor therapy. Acta Biomater 2018;79:37–59 [PubMed: 30165201]
44. Klammert U, Gbureck U, Vorndran E, et al. 3D powder printed calcium phosphate implants for reconstruction of cranial and maxillofacial defects. J Craniomaxillofac Surg 2010;38:565–570 [PubMed: 20206538]
45. Barrère F, van Blitterswijk CA, de Groot K. Bone regeneration: molecular and cellular interactions with calcium phosphate ceramics. Int J Nanomedicine 2006;1:317–332 [PubMed: 17717972]
46. Moore WR, Graves SE, Bain GI. Synthetic bone graft substitutes. ANZ J Surg 2001;71:354–361 [PubMed: 11409021]
47. Kivrak N, Taş AC. Synthesis of calcium hydroxyapatite-tricalcium phosphate (HA-TCP) composite bioceramic powders and their sintering behavior. Journal of the American Ceramic Society 1998;81:2245–2252
48. Smith BT, Shum J, Wong M, et al. Bone Tissue Engineering Challenges in Oral & Maxillofacial Surgery. Adv Exp Med Biol 2015;881:57–78 [PubMed: 26545744]
49. Zhang Z, Ortiz O, Goyal R, et al. Biodegradable polymers. Handbook of Polymer Applications in Medicine and Medical Devices: Elsevier; 2014:303–335
50. Sheikh Z, Najeeb S, Khurshid Z, et al. Biodegradable Materials for Bone Repair and Tissue Engineering Applications. Materials (Basel) 2015;8:5744–5794 [PubMed: 28793533]
51. Moreau JL, Caccamese JF, Coletti DP, et al. Tissue engineering solutions for cleft palates. J Oral Maxillofac Surg 2007;65:2503–2511 [PubMed: 18022477]
52. Coelho PG, Jimbo R. Osseointegration of metallic devices: current trends based on implant hardware design. Arch Biochem Biophys 2014;561:99–108 [PubMed: 25010447]
53. Miranda P, Pajares A, Saiz E, et al. Mechanical properties of calcium phosphate scaffolds fabricated by robocasting. J Biomed Mater Res A 2008;85:218–227 [PubMed: 17688280]
54. Dong J, Uemura T, Shirasaki Y, et al. Promotion of bone formation using highly pure porous beta-TCP combined with bone marrow-derived osteoprogenitor cells. Biomaterials 2002;23:4493–4502 [PubMed: 12322969]
55. Tee BC, Desai KG, Kennedy KS, et al. Reconstructing jaw defects with MSCs and PLGA-encapsulated growth factors. Am J Transl Res 2016;8:2693–2704 [PubMed: 27398152]
56. Yuan J, Cui L, Zhang WJ, et al. Repair of canine mandibular bone defects with bone marrow stromal cells and porous beta-tricalcium phosphate. Biomaterials 2007;28:1005–1013 [PubMed: 17092556]
57. Zhou H, Deng Y, Bi X, et al. Orbital wall repair in canines with beta-tricalcium phosphate and induced bone marrow stromal cells. J Biomed Mater Res B Appl Biomater 2013;101:1340–1349 [PubMed: 23687075]
58. Kazemi M, Dehghan MM, Azami M. Biological evaluation of porous nanocomposite scaffolds based on strontium substituted beta-TCP and bioactive glass: An in vitro and in vivo study. Mater Sci Eng C Mater Biol Appl 2019;105:110071 [PubMed: 31546377]

59. Shimizu A, Tajima S, Tobita M, et al. Effect of Control-released Basic Fibroblast Growth Factor Incorporated in beta-Tricalcium Phosphate for Murine Cranial Model. Plast Reconstr Surg Glob Open 2014;2:e126 [PubMed: 25289319]

60. Han SH, Jung SH, Lee JH. Preparation of beta-tricalcium phosphate microsphere-hyaluronic acid-based powder gel composite as a carrier for rhBMP-2 injection and evaluation using long bone segmental defect model. J Biomater Sci Polym Ed 2019;30:679–693 [PubMed: 30939993]

61. Tao ZS, Zhou WS, Wu XJ, et al. Single-dose local administration of parathyroid hormone (1–34, PTH) with beta-tricalcium phosphate/collagen (beta-TCP/COL) enhances bone defect healing in ovariectomized rats. J Bone Miner Metab 2019;37:28–35 [PubMed: 29392472]

62. Wang L, Fan H, Zhang ZY, et al. Osteogenesis and angiogenesis of tissue-engineered bone constructed by prevascularized beta-tricalcium phosphate scaffold and mesenchymal stem cells. Biomaterials 2010;31:9452–9461 [PubMed: 20869769]

63. Xie Z, Yan D, Zhou Q, et al. The fast degradation of β-TCP ceramics facilitates healing of bone defects by the combination of BMP-2 and Teriparatide. Biomed Pharmacother 2019;112:108578–108578 [PubMed: 30784943]

64. Auston DA, Feibert M, Craig T, et al. Unexpected radiographic lucency following grafting of bone defects with calcium sulfate/tricalcium phosphate bone substitute. Skeletal Radiol 2015;44:1453–1459 [PubMed: 26081807]

65. Anker CJ, Holdridge SP, Baird B, et al. Ultraporous beta-tricalcium phosphate is well incorporated in small cavitary defects. Clin Orthop Relat Res 2005:251–257

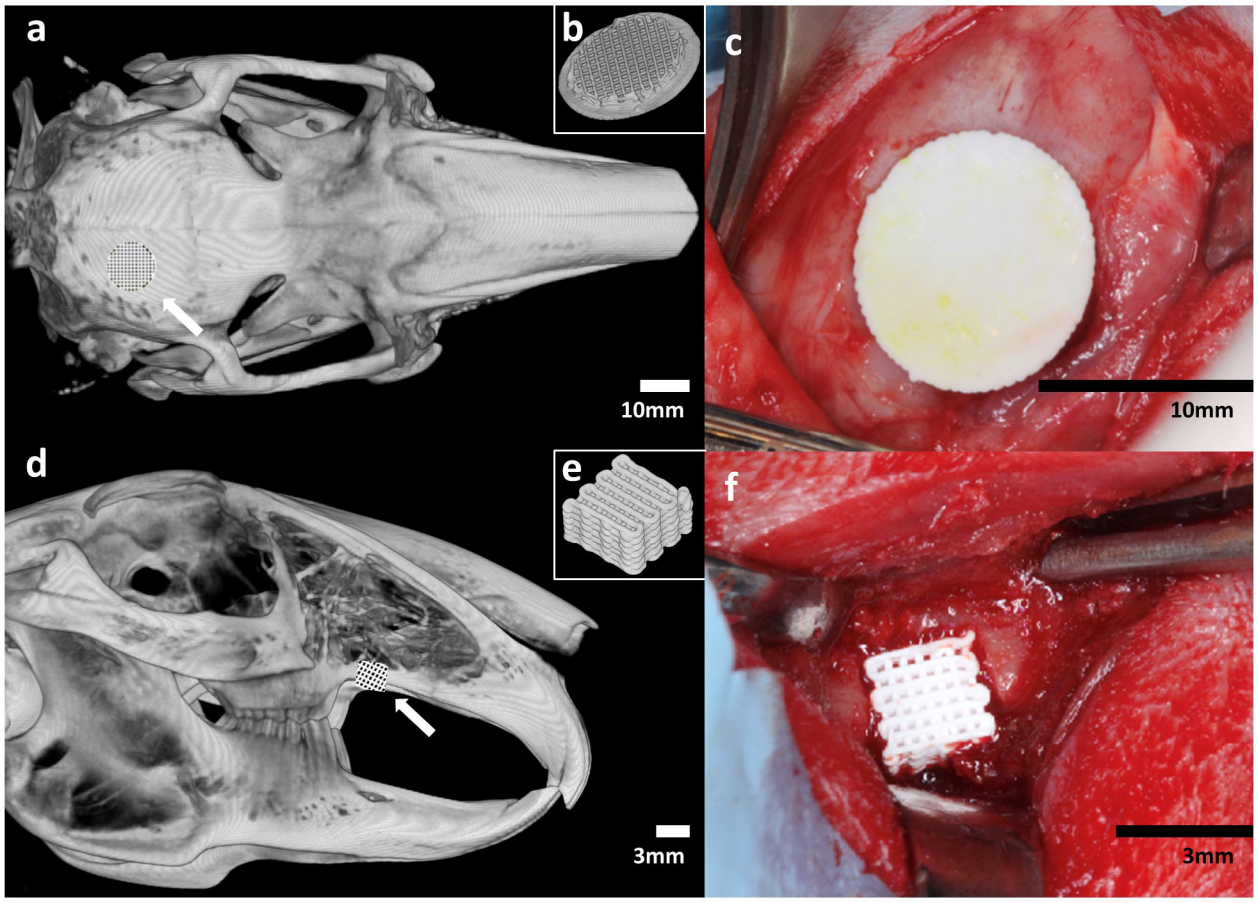

Figure 1.

(a) Schematic of location of unilateral calvarial defect. **(b)** Inferior view of 3D diagram of printed calvarial scaffold. **(c)** Intraoperative image of fit-and-fill reconstruction of calvarial defect with scaffold. **(d)** Schematic of location of unilateral alveolar defect. **(e)** 3D diagram of printed alveolar scaffold. **(f)** Intraoperative image of fit-and-fill reconstruction of alveolar defect with scaffold.

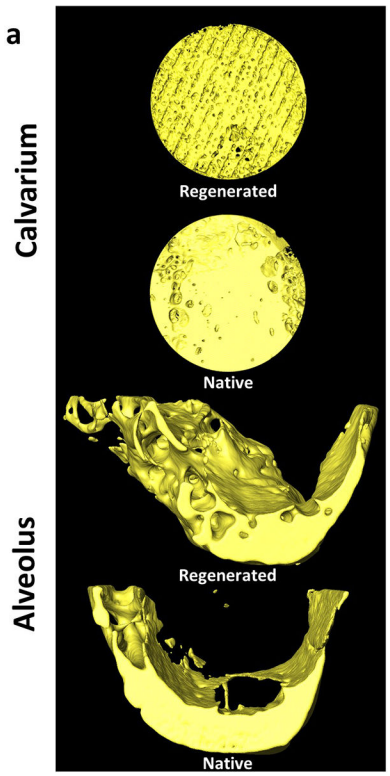

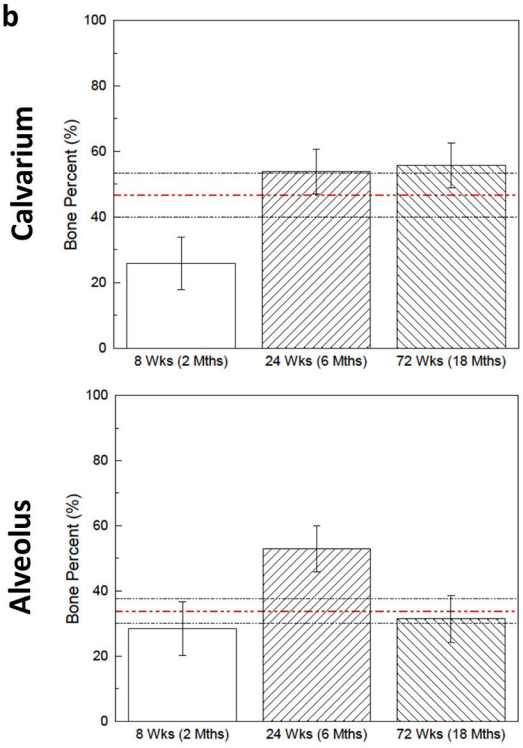

c

Calvarium

		p-value
18 Months	2 Months	**<0.001**
18 Months	6 Months	**0.705**
18 Months	Native bone	**0.064**

Alveolus

		p-value
18 Months	2 Months	**0.566**
18 Months	6 Months	**<0.001**
18 Months	Native bone	**0.337**

Figure 2.

(a) 3D reconstructions of scaffold-regenerated bone (yellow) at 18 months *in vivo* demonstrate regeneration across entire span of calvarial and alveolar defects, with morphology comparable to contralateral un-operated native bone. **(b)** Volumetric analysis of shows comparable bone volume fraction regenerated by scaffold compared to native bone (red dashed line; black dashed lines are 95% confidence intervals) at 18 months in both **(c)** calvarium and alveolus ($p = 0.064$ and $p = 0.337$, respectively). Error bars are 95% confidence intervals. Bone Percent = Bone Volume/Total Volume.

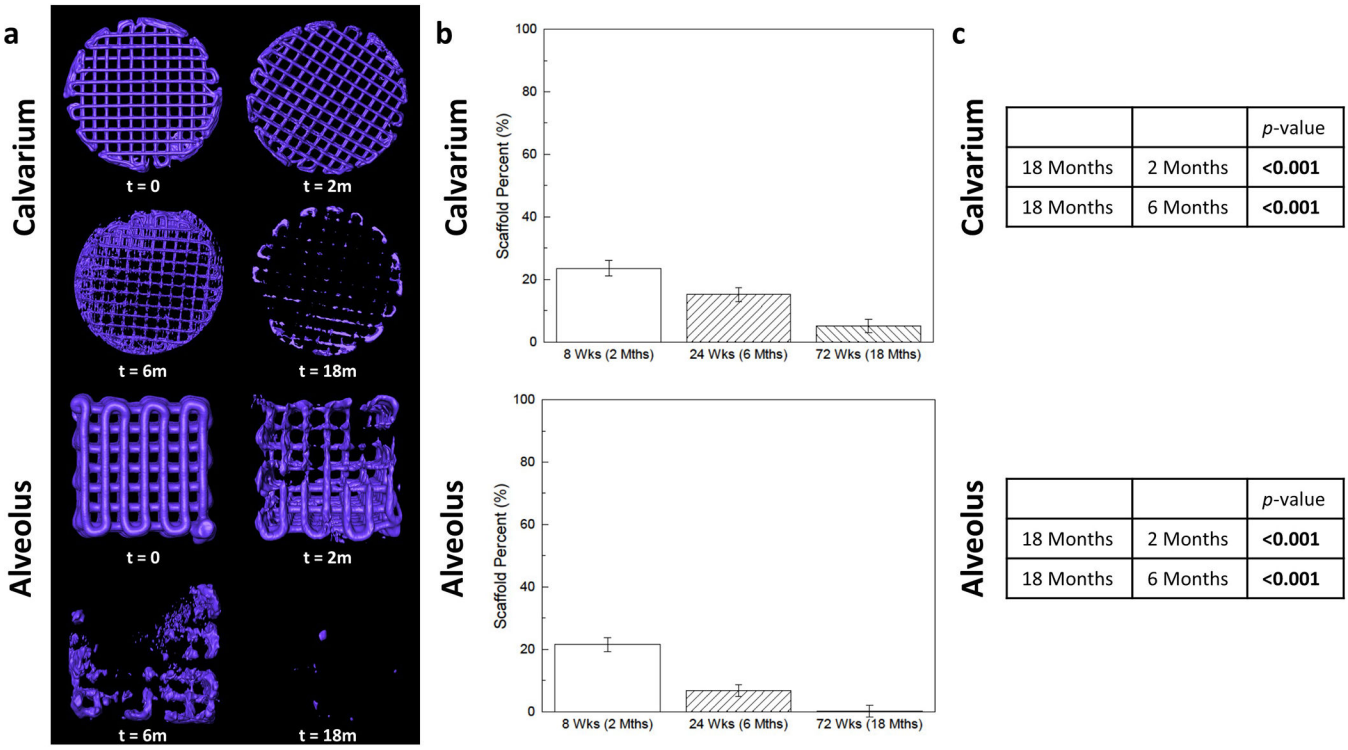

		p-value
18 Months	2 Months	**<0.001**
18 Months	6 Months	**<0.001**

		p-value
18 Months	2 Months	**<0.001**
18 Months	6 Months	**<0.001**

Figure 3.

(a) 3D reconstructions of scaffold (purple) and **(b)** volumetric analysis demonstrate significant degradation of the scaffold from 2 months to 18 months in both **(c)** calvarium and alveolus ($p < 0.001$ between all timepoints). Error bars are 95% confidence intervals Scaffold Percent = Bone Volume/Total Volume.

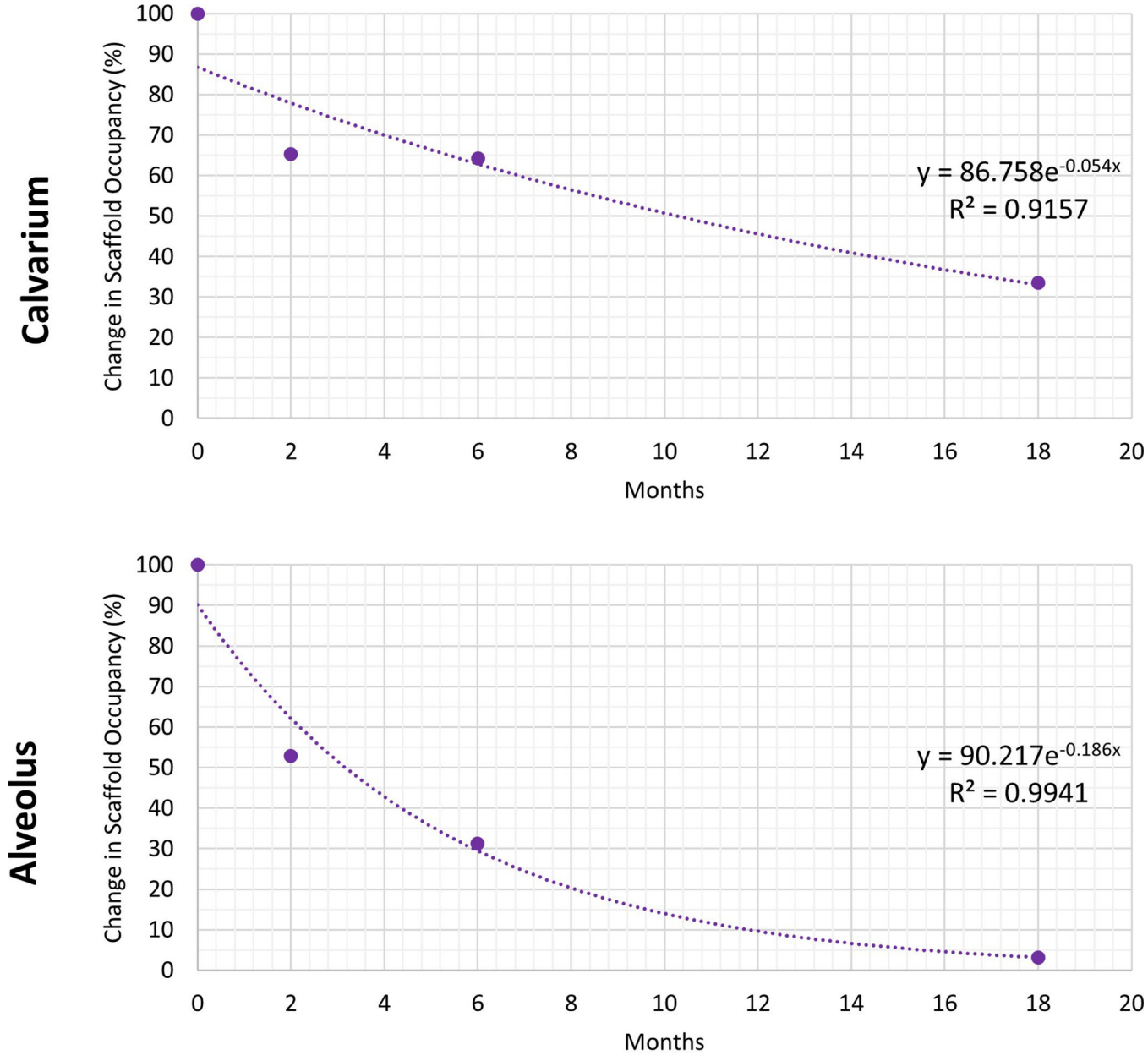

Figure 4.

Degradation kinetics analysis of scaffold over 18 months used to calculate annual degradation rate of β-TCP in calvarium and alveolus (54.6% and 90.5%, respectively). Change in Scaffold Occupancy = (Scaffold Percent at time *t*/(Scaffold Percent at time *t-1*).

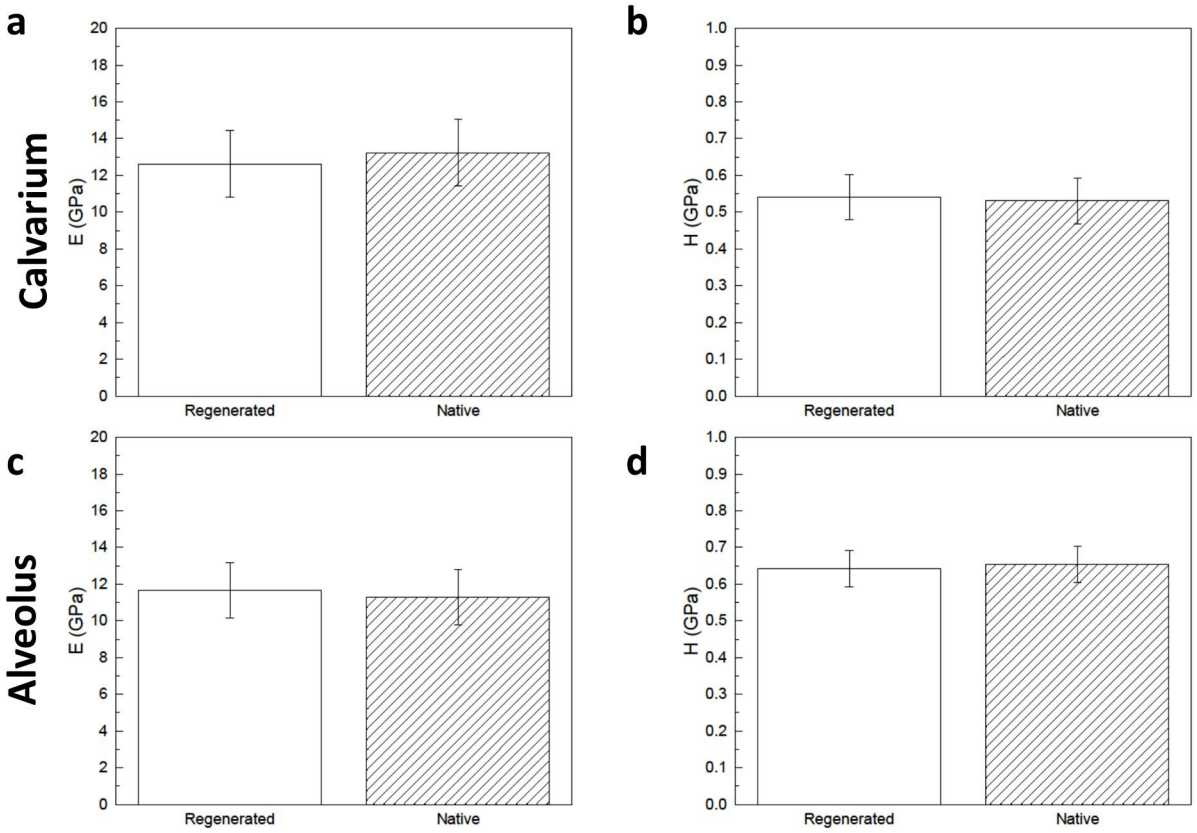

Figure 5.

Elastic modulus (E) of **(a)** calvarial and **(c)** alveolar scaffold-regenerated bone show no difference compared to that of native control. Hardness (H) of **(b)** calvarial and **(d)** alveolar scaffold-regenerated bone show no difference compared to that of native control. Error bars are 95% confidence intervals.

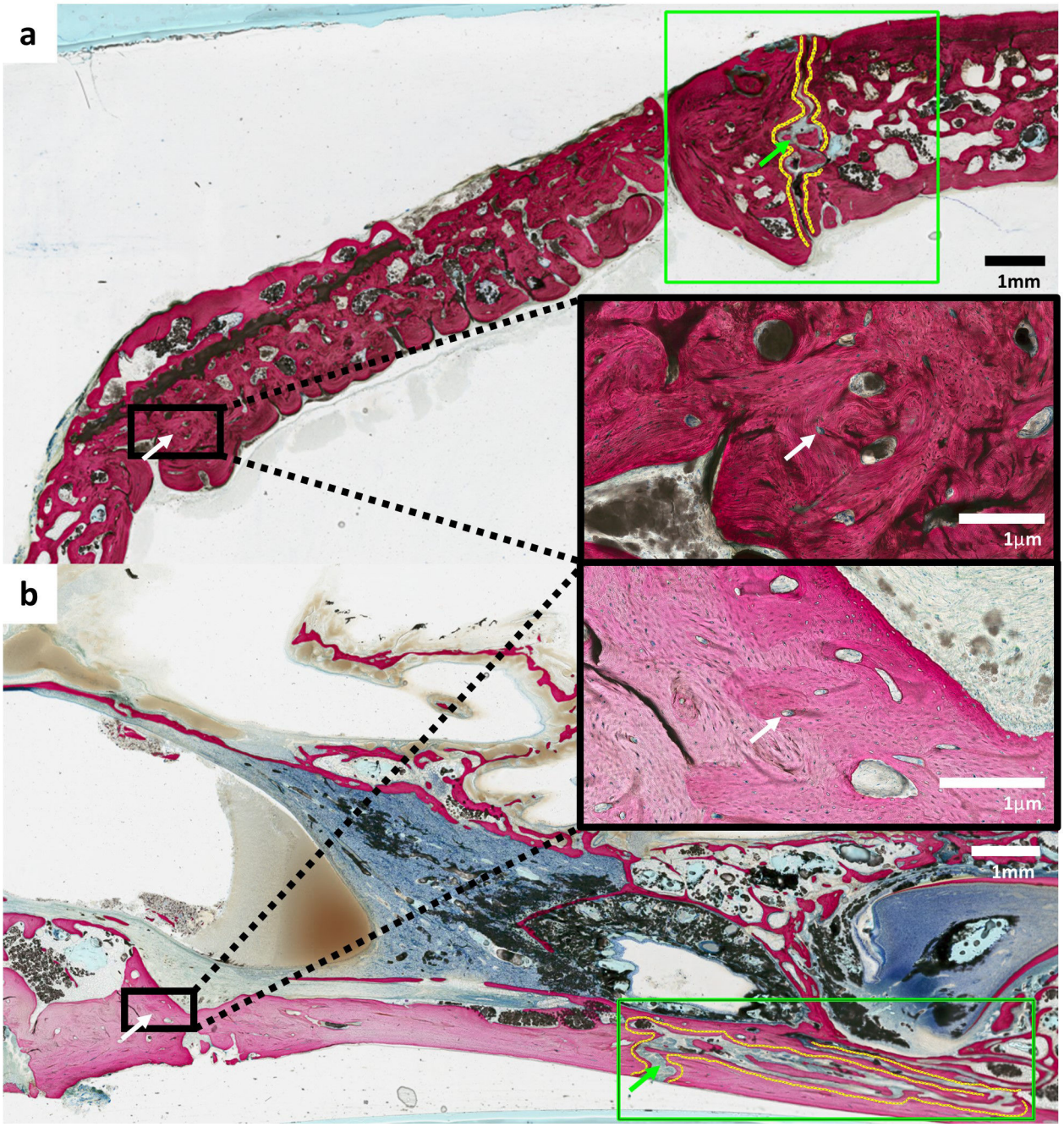

Figure 6.

Non-decalcified histology of **(a)** calvarial and **(b)** alveolar scaffolds at 18 months show blood vessels stained with Stevenel's blue with surrounding organized bone (white arrows) and patent sutures without evidence of disruption or premature fusion (green arrows) adjacent to sites of reconstruction. No evidence of ectopic bone formation or inflammatory cells were visualized in all samples.

TABLE 1.

Review of Tissue Engineering Methods to Alter the Degradation Kinetics of β-TCP

Year	Author	Species	Anatomic Location	Construct/Method	Experimental Model	Degradation Analysis
2002	Dong et al	7-wk-old Fisher rats	Back	β-TCP scaffolds seeded with BMSCs either cultured in osteogenic medium or incubated in nonosteogenic medium	Implantation of multiple blocks into separate subcutaneous pouches	On histology at 24 wk, control scaffolds resorbed slower than experimental scaffolds because of decreased bone formation and increased exposure to resorptive soft tissue.
2007	Yuan et al	18-mo-old mongrel dogs	Mandible	β-TCP scaffolds seeded with osteogenically induced BMSCs	30-mm segmental defect fixed with titanium plate and filled with scaffold	On plain radiograph and histology at 32 wk, scaffold almost completely degraded.
2010	Wang et al	12-wk-old New Zealand rabbits	Femur	β-TCP scaffolds seeded with osteogenically differentiated BMSCs and prevascularized with insertion of femoral vascular bundle into the side groove of scaffold	15-mm segmental defect fixed with titanium plate and filled with scaffold	On histology at 12 wk, most of the prevascularized scaffold degraded faster than non-prevascularized scaffold.
2013	Zhou et al	1- to 2-y-old beagle dogs	Medial orbital wall	β-TCP scaffolds seeded with osteogenically induced BMSCs	10-mm-diameter round full-thickness defect filled with scaffold	On micro-CT and histology, induced scaffolds degraded faster than both noninduced and unseeded scaffolds. BMD measurements of the experimental group were similar to those of normal bone at 3 mo.
2014	Shimizu et al	10-wk-old Sprague-Dawley rats	Cranium	β-TCP scaffolds coated in bFGF-containing gelatin hydrogel	Bilateral 4-mm-diameter full-thickness defects filled with scaffold	On CT and histology at 4 wk, bFGF-coated scaffolds degraded faster than noncoated scaffolds.
2016	Tee et al	4-mo-old domestic pigs	Mandible	β-TCP scaffolds seeded with BMSCs and integrated with PLGA microspheres containing BMP-2	Bilateral 3.5-mm segmental defect sealed by either fibrin sealant or fibrin sealant with barrier membrane	On volumetric analysis and histology at 12 wk, β-TCP degradation decreased when integrated with BMSC and growth factor or with barrier containment.
2019	Han et al	Sprague-Dawley rats	Fibula	β-TCP microsphere-hyaluronic acid powder gel composite loaded with rhBMP-2	5-mm segmental defect filled with composite	On histology at 9 wk, fewer loaded composite remnants were noted compared with unloaded composite remnants.
2019	Kazemi et al	5- to 6-mo-old New Zealand white rabbits	Calvaria	Strontium substituted β-TCP and bioactive glass (50/50) scaffolds seeded with BMSCs	8-mm-diameter full-thickness defect filled with scaffold	On CT and histology at 5 mo, almost all the cell-loaded scaffold was degraded, whereas bone growth and degradation were seemingly halted within the cell-free scaffold because of fibrous connective tissue surrounding the slow-degrading glass material.
2019	Tao et al	3-mo-old Sprague-Dawley rats	Femur	β-TCP/collagen composite	5-mm segmental defect in ovariectomized rats filled with composite and locally administered with PTH	On histology at 8 wk, the PTH-administered group showed decreased remaining biomaterial compared with the composite-only group.

bFGF, basic fibroblast growth factor; PLGA, poly(lactic-co-glycolic acid); PTH, parathyroid hormone; rhBMP-2, recombinant human-bone morphogenetic protein-2.